To the Graduate Council:

I am submitting herewith a thesis written by A. L. Nasser entitled "Radiographic Image Edge Detection Techniques: Experiments on a Rocket Nozzle Simulator." I have examined the final copy of this thesis for form and content and recommend that it be accepted in partial fulfillment of the requirements for the degree of Master of Science, with a major in Engineering Science.

R A Belz

Ronald Belz, Major Professor

We have read this thesis and recommend its acceptance:

Jack H. Hansen

Charles C. Limbaugh

Accepted for the Council:

Cw Minkel

Vice Provost and
Dean of The Graduate School

STATEMENT OF PERMISSION TO USE

In presenting this thesis in partial fulfillment of the requirements for a Master's degree at The University of Tennessee, Knoxville, I agree that the Library shall make it available to borrowers under rules of the Library. Brief quotations from this thesis are allowable without special permission, provided that accurate acknowledgment of the source is made.

Permission for extensive quotation from or reproduction of this thesis may be granted by my major professor, or in his absence, by the Head of Interlibrary Services when, in the opinion of either, the proposed use of the material is for scholarly purposes. Any copying or use of the material in this thesis for financial gain shall not be allowed without my written permission.

Signature _[signature]_

Date 8/15/98

RADIOGRAPHIC IMAGE EDGE DETECTION TECHNIQUES: EXPERIMENTS ON A ROCKET NOZZLE SIMULATOR

A Thesis

Presented for the

Master of Science

Degree

The University of Tennessee, Knoxville

A. L. Nasser

December 1988

ABSTRACT

The purpose of this thesis is to study the application of edge detection techniques to radiographic images. Image edge detection is the first step in enhancing analysis capabilities from visual analysis to radiographic image measurement with known accuracy. Edge detection will make tasks like measurement of rocket nozzle throat erosion or propellant burn rate possible.

Five detection techniques were considered as candidate detectors for radiographic image analysis. These techniques were all tested using the same radiographic images and their results were compared.

This study was focused on measurement of rocket nozzle throat erosion. Since data from an actual rocket firing were not available, a nozzle throat simulator was designed and constructed. X-ray data of the simulator provided exactly known "throat" or hole diameters which were used in evaluation of the different detection techniques.

For the conditions examined here, the K-means combined with Sobel gradient preprocessing edge detection technique was found to be superior to the others evaluated. Results from this procedure produced error levels less than 0.125 inches for hole measurements ranging from approximately 1 to 3 inches.

TABLE OF CONTENTS

LIST OF TABLES

LIST OF FIGURES

CHAPTER I

INTRODUCTION

X rays are commonly used in solid rocket motor diagnostics to provide images of the internal components. An X-ray imaging system, shown schematically in Figure 1, consists of an X-ray source and an X-ray detector. As the X rays traverse the object being radiographed, they may be scattered or absorbed depending on their energy [1]. The black and white X-ray images are dependent upon the X-ray attenuation coefficient of the object, which to a large extent depends on its density and atomic number. X-ray images resulting from energy absorbed by a denser object or higher atomic number medium are indicated by darker images, or lower gray-level intensity values. The less X-ray energy to reach the detector, the darker the image. Scattered photons do not reach the detector along their initial direction of travel (as though it were absorbed), but will instead add energy to another portion of the image slightly displaced from the original direction of travel. Therefore, instead of casting a sharp shadow image on the detector, the scattered radiation forms a broad, diffuse distribution on the detector reducing the contrast of the image formed by unscattered radiation.

Image analysis (or object measurement for this effort) is dependent on the quality of edge definition in the image. Images with easily defined edges can be detected and measured with little effort. Images of low contrast or blurred object edges require

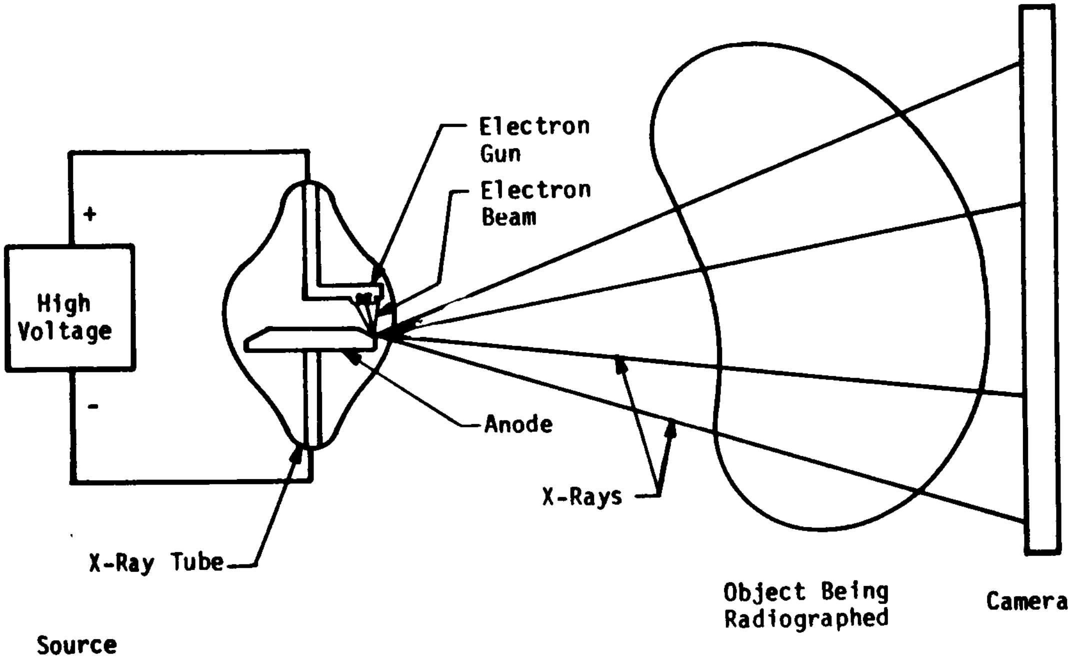

Figure 1. Typical imaging system.

preprocessing or more sophisticated edge detection techniques to improve the uncertainties in determining edge locations.

X-ray radiography is used to analyze the performance of a solid rocket motor during testing at simulated altitude conditions in test chambers like those at the Arnold Engineering Development Center (AEDC). Current imaging technology at AEDC is limited to analysis by human visual inspection which subjects accuracy to unknown errors. Development of an edge detection procedure for radiographic image analysis is the first step in upgrading current technological capabilities for items like analysis of rocket nozzle throat erosion and propellant burn-rate measurement.

This research concentrates on edge detection methods for the analysis of nozzle throat erosion. As shown in Equation (1), the throat dimensions can have profound effects on rocket performance, and development of real-time throat dimension determination can upgrade test-data quality and test-article performance analysis.

Performance of a solid rocket nozzle is characterized by specific impulse; defined by

$$I_{sp} = A_t * C_f * P_c/\dot{W}, \tag{1}$$

where A_t is the throat area, C_f is the thrust coefficient, P_c is the chamber pressure, and $\dot{W}$ is exhaust mass flow rate. As the nozzle throat erodes (due to exhaust dynamics and high temperatures), it becomes larger. Although performance would appear to increase (from inspection of Equation (1)), it is generally found to decrease. This is because the thrust coefficient, C_f, is a function of nozzle throat to exit area ratio, and a small increase in throat area will correspond to a relatively large decrease in C_f (and a consequent decrease in I_{sp}). In fact, even a one-percent change in throat area could correspond to as much as a three-percent decrease in overall rocket performance (I_{sp}). Therefore, the ability to recognize and measure such an erosion process during a static test could impact early rocket motor development.

The purpose of this study is to investigate edge detection techniques which could be used to measure solid rocket nozzle images produced by radiographic instrumentation. Since rocket nozzle erosion data were not available for these analyses, a solid rocket nozzle simulator was designed and constructed, of which radiographic images could be made. Using this simulator, measurements of various hole sizes were made, from which judgments about edge detection procedures were evaluated.

The candidate edge detection techniques selected for study are listed below and discussed in Chapter II:

1. Thresholding
2. Pixel Clustering--K-Means
3. Pixel Clustering--ISODATA
4. Gradient
5. Laplacian

The radiographic experiment setup from which throat simulator images were made is explained in Chapter III. Chapter IV presents the results of using specific edge detector techniques on X-ray images, and Chapter V summarizes the results.

CHAPTER II

DETECTION TECHNIQUES

The problem of edge detection can be explained by considering a broad field image including some object, and noting that the object is observed in the ideal case as an intensity discontinuity. For example, in an image of the moon and surrounding sky, the moon will appear light and the sky as dark. The overall image can be represented by rows and columns of gray levels. Each gray-level element or pixel represents the smallest spatial unit making up the overall image. As a row of image pixel (discrete image points) intensities is scanned, the moon's edge can be located when a transition from dark (low pixel intensity) to light (high pixel intensity) is noted (or vice versa). Gray scale values may range from 0 for black to 255 for white when a gray scale of 256 discrete values is used. Figure 2 shows an example of a light object against a dark background. A profile of pixel intensity values taken across the image (along the line indicated in Figure 2a) is shown in Figure 2b. A straight line was drawn between discrete pixel points in the figure, but better resolution (more pixels) might alter this presentation. As the image is scanned from left to right, the first object edge is located between pixels 3 and 4 and the second between pixels 8 and 9. The edges, for this case, are easily identified. However, if the image was extremely noisy, the contrast poor, or the edge blurred over several pixels, identification of the edge would be more

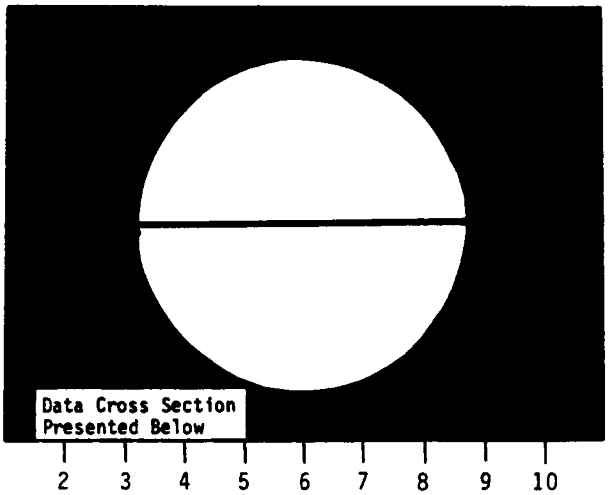

a. Image data

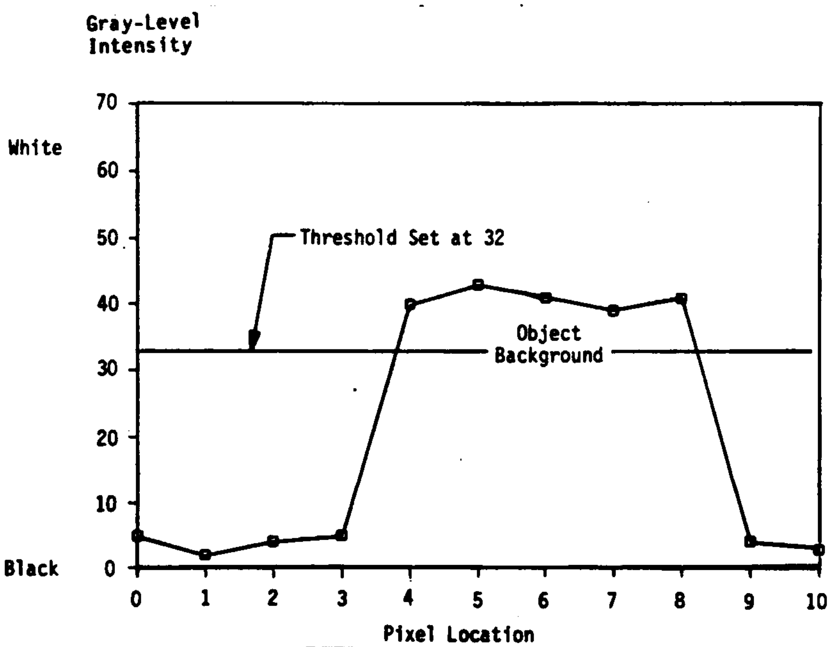

b. Profile of image data

Figure 2. Typical image.

difficult. Edge detection techniques have the potential to identify edges from these degraded images.

Five edge detection techniques are presented in the following sections. Each technique is evaluated with image profiles similar to the example presented in Figure 2. Because of the similarity between intensity changes for transition from background to object and object to background, only the first transition edge is examined in the following discussion. In the example presented in Figure 2, only pixel loxations 0 through 6 are discussed.

Thresholding

A gray-level (image pixel intensity) threshold value is established (Figure 2); and once this threshold value is exceeded, the edge is established. Gonzalez and Wintz call this the "Gray-Level Thresholding" technique for edge detection [2]. In most instances, the threshold value will be determined based upon prior knowledge about the principal brightness regions or a percentage increase in intensity [3]. A histogram can be used to determine an appropriate threshold level for a similar set of images. Figure 3a presents an image profile containing an edge with its histogram in Figure 3b. The histogram shows that the profile has nearly a bimodal gray-level distribution with most pixels located at about gray-level 25 or 50. As shown in Figure 3, the edge pixel is that nearest 37.5 or half the gray-level distance between the two mean intensities (pixel location 13 as indicated in Figure 3c). This illustrates that for this technique, a nearly bimodal gray-level image pixel distribution is

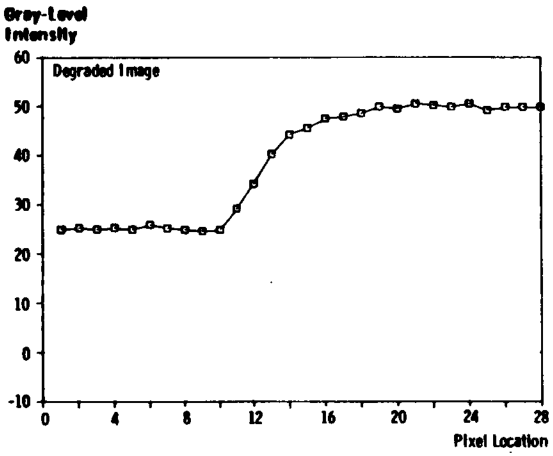

a. Partial image profile

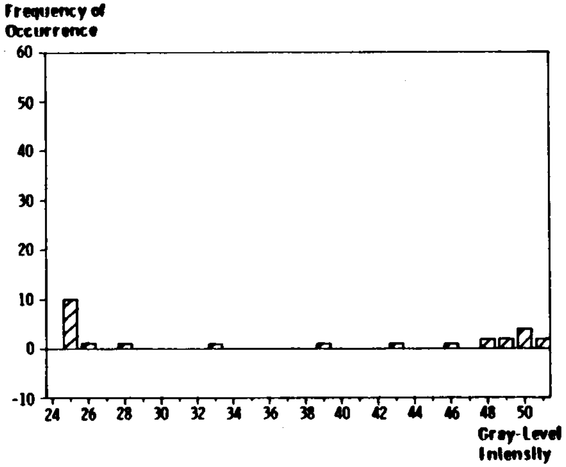

b. Histogram

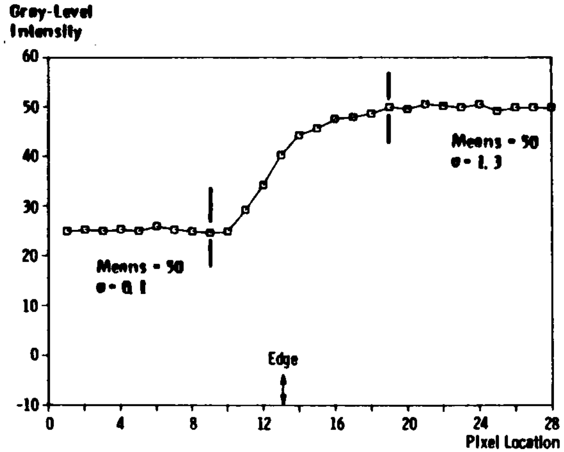

c. Threshold result

Figure 3. Example of thresholding.

necessary for edge detection in order to adequately define the light and dark regions. Blurring, which produces more than two primary gray levels in the image histogram, can make discerning object from background pixels impossible since only two gray-level regions are expected.

Pixel Clustering--K-Means

Pixel clustering detects an edge by grouping adjacent image pixels with similar traits or characteristics. K-means is a specific pixel clustering technique as described by Tou and Gonzalez [4]. An image data profile, such as that shown in Figure 4a, is arbitrarily divided into two pixel groups (A and B). In this example, the A side consists of pixels 1 through 5, and the B side consists of pixels 6 through 29. The distribution of the number of pixels about their mean in each group will be unequal initially, and the cluster groupings will be adjusted during the iterative process as described in the following paragraph.

A mean gray-level value (z) is calculated for each side by

$$z = 1/N \sum_{i=1}^{N} x_i, \tag{2}$$

where N is the total number of pixels included in each side, and x_i is the gray-level intensity value for each pixel. Then a performance index given by the total pixel variance is calculated based on the current pixel groupings (A and B). This index is calculated by

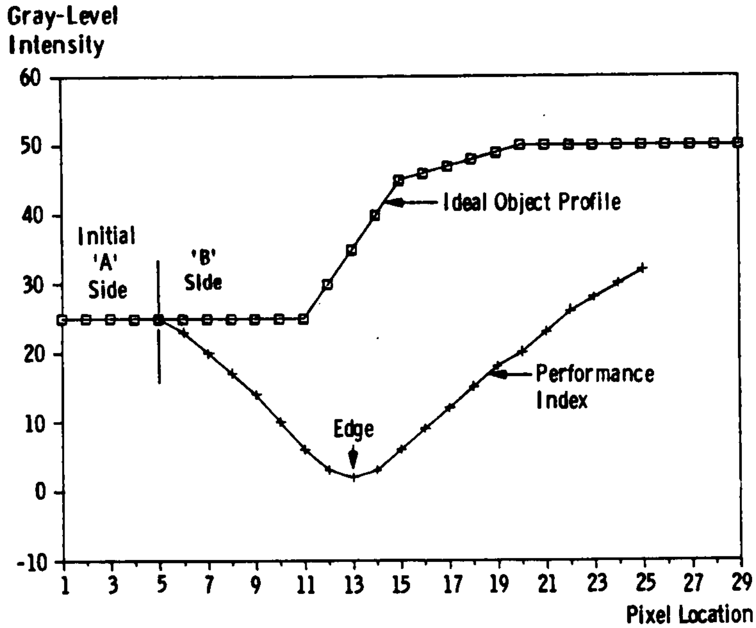

a. Ideal image

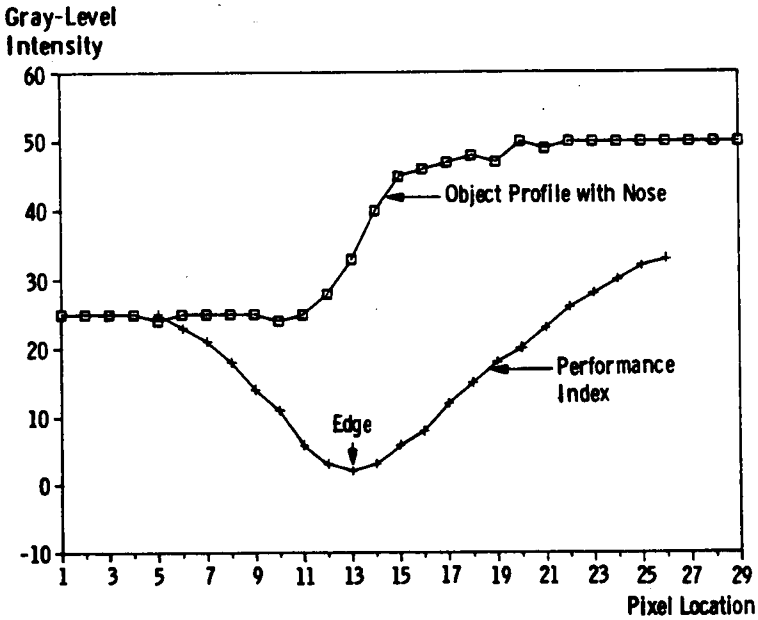

b. Noisy image

Figure 4. Example of K-means.

$$J = \sum_{Nc} \sum_{N} | x_i - z |^2, \tag{3}$$

where Nc is the total number of clusters (two in this case). For the initial configuration, the performance index is about 25, as shown in Figure 4a. Next, pixel location 6 is added to the A side and deleted from B-side calculations. The performance index is recalculated and is now shown to be slightly less than 25, as indicated in the same figure. This process of adjusting pixel groupings is repeated, and corresponding performance index results are calculated. The figure demonstrates that at pixel location 13, the performance index is minimized. This means that the total gray-level variance from grouping pixels into two clusters (A and B) is lowest when cluster A contains pixels 1 through 13 and the remaining pixels are assigned to cluster B. K-means analysis for this profile locate the image edge at pixel 13.

To establish the effect of an image noise level less than that found in the actual throat simulator data on K-means results, the profile presented in Figure 4a was slightly degraded by averaging four slightly different consecutive hole profiles. Analysis of the degraded image produced identical pixel groupings (Figure 4b) thus indicating that image noise had no effect on K-means results. The image edge is still at location 13.

Pixel Clustering--ISODATA

Iterative Self-Organizing Data Analysis Techniques (ISODATA) is another specific clustering algorithm and is similar to the

K-means technique described previously [4]. Using the same image profile as presented earlier in Figure 4 during K-means discussions, Figure 5 presents results of typical ISODATA analysis. First data were arbitrarily divided into two initial clusters (Figure 5a), and a mean and standard deviation for the gray-level intensities in each was calculated. For this example, a standard deviation threshold was arbitrarily set at 5. This is a reasonable threshold since the mean gray-level difference between the maximum light (50) and minimum dark (25) regions is 25, and a threshold of 5 will place the edge between a gray level of 30 and 45. Any pixel grouping with a standard deviation above this threshold is subdivided into two equal-sized clusters. In Figure 5a, cluster 2 has a deviation of 9.3. Thus, as shown in Figure 5b, it is divided into two new pixel groupings (2A and 2B) with respective deviations of 13.7 and 0. Because of the 5 pixel threshold criteria, cluster 2A is divided into clusters 2A1 and 2A2, but the threshold of 5 is still exceeded by cluster 2A1. Since the desired number of clusters is two, and four clusters have already been established in Figure 5c, no additional subdividing is allowed by ISODATA definition. Instead, the total number of clusters is reduced to two by combining cluster 1 and 2A1, and 2A2 and 2B. A mean and standard deviation is calculated for each grouping and now both clusters meet the 5 gray-level threshold limit. Therefore, no additional adjustments will be made to cluster assignments. The ISODATA result for this image profile analysis locates an edge at pixel 14 (Figure 5d).

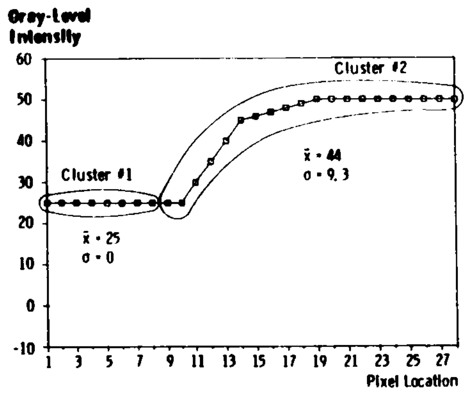

a. Initial

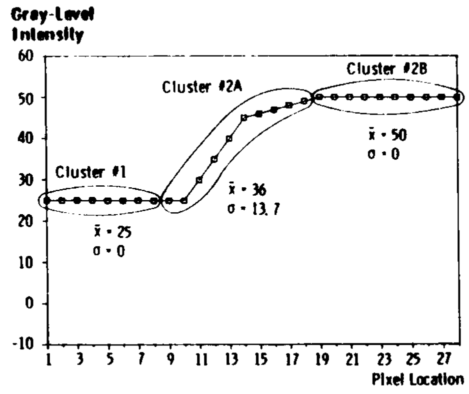

b. First pass

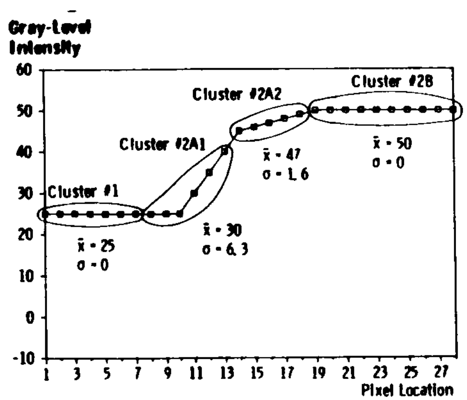

c. Second pass

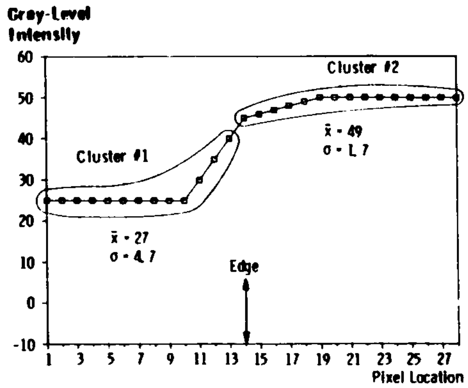

d. Third pass

Figure 5. Example of ISODATA on an ideal image.

From the preceding discussion, it is apparent that alteration of ISODATA initial conditions will change the resulting edge location. However, since changes in edge location of the first and second edges are always relative for this process, alteration in initial conditions will not matter. To determine the effect of image noise on ISODATA's capability to determine an edge, the same degraded image (Figure 4) used to test the K-means procedure will be analyzed. Figure 6 shows results from the ISODATA technique for analysis of the degraded image. The profile is clustered into two groups initially, then three and four. However, the same final end product of just two pixel groupings is the result. This verifies that ISODATA is not hampered by a slight amount of image noise.

Gradient

An image enhancement technique commonly used for edge detection is the gradient [5]. Given a function f(x,y), the gradient of f at coordinates (x,y) is defined as the vector,

$$G\,[f(x,y)] = \begin{bmatrix} \frac{\delta f}{\delta x} \\ \\ \frac{\delta f}{\delta y} \end{bmatrix} . \tag{4}$$

Gonzalez and Wintz [2] indicate two important properties of the gradient, G [f(x,y)]:

1. the vector G [f(x,y)] points in the direction of the maximum rate of change of the function f(x,y);

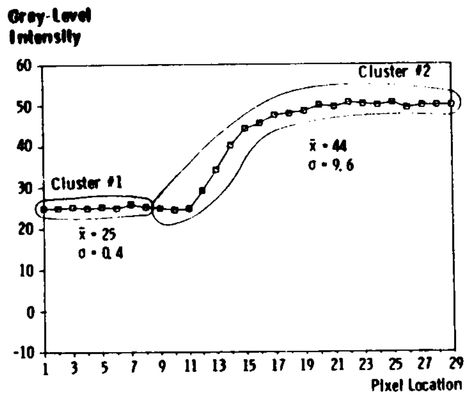

a. Initial

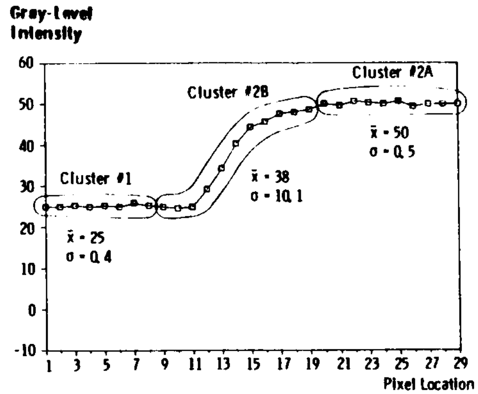

b. First pass

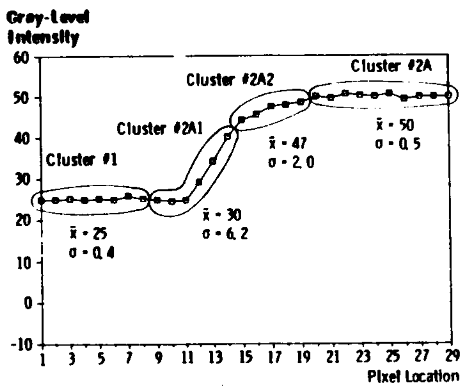

c. Second pass

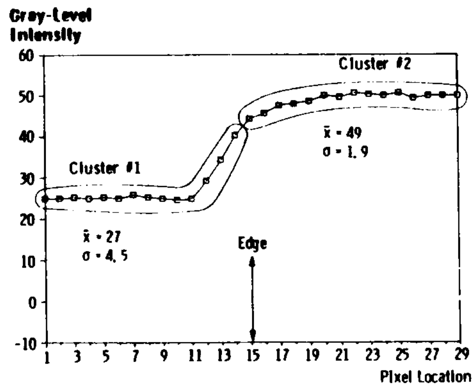

d. Third pass

Figure 6. Example of ISODATA on a noisy image.

2. the magnitude of G [f(x,y)] equals the maximum rate of change of f(x,y) per unit distance in the direction of G, as given by

$$\text{mag}\ [G] = \left\{ \left(\frac{\delta f}{\delta x} \right)^2 + \left(\frac{\delta f}{\delta y} \right)^2 \right\}^{\frac{1}{2}}. \tag{5}$$

In image processing, the gradient in Equation (5) can be approximated by a digital mask using approximations to the partial derivatives $\frac{\delta f}{\delta x}$ and $\frac{\delta f}{\delta y}$. Reference 2 explains that a digital mask (or template) is an array designed to detect an invarient regional property within the image. Each entry in the array contains a weighting factor for the pixel in that relative location. The center of the mask is moved around the image pixel by pixel. At each position, every pixel within the mask is multiplied by the corresponding entry of the mask, then all values within the mask are added together. These approximations in image processing (IP) are often accomplished by the use of a process called a digital mask.

Various digital masks have been proposed to approximate these differential operators, and mask weights for the different approximations always sum to zero. In image processing, such convolution of a properly designed mask will result in the gradient of the image.

The simplest proposal uses 2 x 2 masks for gradient approximation [6], yielding

$$\begin{aligned} \dot{f}_y &= f_{i,j+1} - f_{i,j} \\ \dot{f}_x &= f_{i+1,j} - f_{i,j}. \end{aligned} \tag{6}$$

This is derived for $\dot{f}_x$ by expanding a function f in a first-degree Taylor polynomial about a point x_i and evaluating x_{i+h}:

$$f(x_{i+h},y) = f(x_i,y) + f'(x_i,y)h + 1/2*f''(\beta,y)h. \qquad (7)$$

Solving for the first derivative of f and assuming the second derivative term is negligible, this becomes

$$f'(x_i) = (f(x_{i+h}) - f(x_i))/h. \qquad (8)$$

Therefore, the $\dot{f}_x$ portion of the mask is the resultant for h = 1 (and $\dot{f}_y$ is derived similarly). These masks can be written symbolically as

$$\dot{f}_y: \begin{matrix} -1 & 0 \\ 1 & 0 \end{matrix} \quad \text{and} \quad \dot{f}_x: \begin{matrix} -1 & 1 \\ 0 & 0. \end{matrix} \qquad (9)$$

These are overlays that, when convolved with the image, result in the gradient. However, these masks are not produced by normal matrix manipulations.

Prewitt states that a more precise estimate is obtained by fitting a quadratic surface over a 3 x 3 neighborhood of pixels by least squares, and then computing the gradient for the fitted surface [6]. The masks are

$$\dot{f}_y: \begin{matrix} 1 & 0 & -1 \\ 1 & 0 & -1 \\ 1 & 0 & -1 \end{matrix} \quad \text{and} \quad \dot{f}_x: \begin{matrix} 1 & 1 & 1 \\ 0 & 0 & 0 \\ -1 & -1 & -1 \end{matrix} \qquad (10)$$

These are shown pictorially in Figure 7a and are referred to as the Prewitt mask [5]. Derived in the same manner, the Sobel mask

-1	0	1
-1	0	1
-1	0	1

$\partial f/\partial y$

1	1	1
0	0	0
-1	-1	-1

$\partial f/\partial x$

a. Prewitt Mask

-1	0	1
-2	0	2
-1	0	1

$\partial f/\partial y$

1	2	1
0	0	0
-1	-2	-1

$\partial f/\partial x$

b. Sobel Mask

Figure 7. Different techniques for approximating the gradient of an image.

(shown in Figure 7b) weighs the pixels closest in proximity to the one being evaluated more heavily than the others (by a factor of 2).

Figure 8a shows the effectiveness of gradient approximation for image edge analysis. Of course these gradient operators require two-dimension image data input, so these techniques are evaluated with an image area consisting of several image profiles and the result is averaged into a single profile as presented in Figure 8. The gradient result clearly indicates the profile change in slope by the rapid intensity change starting at pixel 9. The image edge is the pixel location indicating the largest intensity in the gradient profile. Since locations 11, 12, and 13 indicate equal intensity values in this case, pixel location 11 is chosen as the edge because of its proximity to the initial rise at pixel 9.

To show that image noise had little effect on the gradient operators results, noise was introduced into the profile shown in Figure 8b. The gradient masks are convolved with four slightly different profiles. The results shown in Figure 8b confirm that neither operator is hampered in locating an image edge by the introduction of noise. Both results show the object edge at pixel location 12.

Since both Prewitt and Sobel yield the same results for both images, only the Sobel operator was used to analyze subsequent nozzle simulator data. The Sobel procedure was chosen over the Prewitt because of the higher intensity readings it produces at the edge locations as shown in Figure 8.

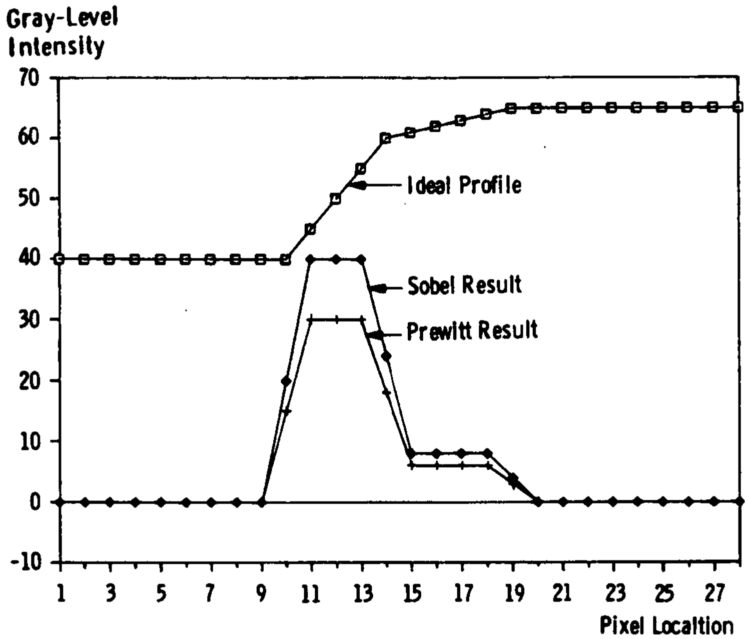

a. Ideal image

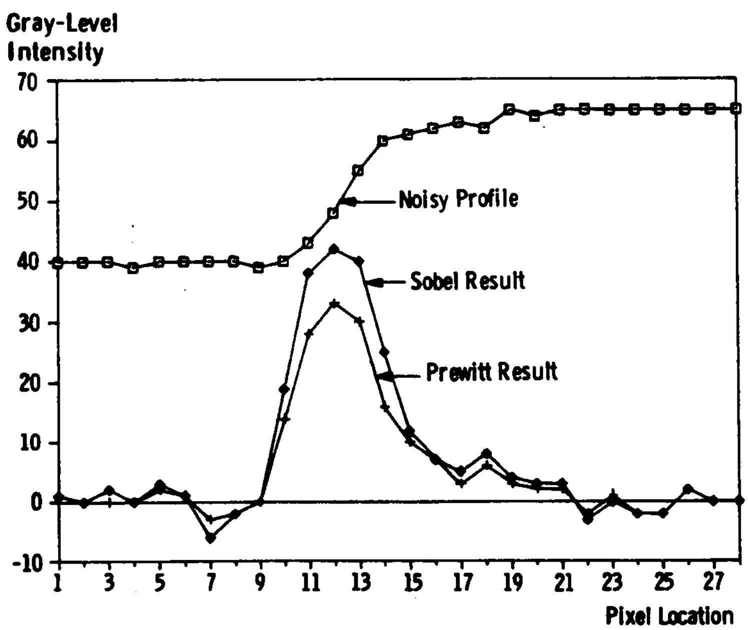

b. Noisy image

Figure 8. Example of gradient approximations.

Laplacian

The Laplacian has historically been used as a means for detecting image edges by analysis of the 2nd derivative. The Laplacian of a two-variable function f(x,y) is defined as

$$\nabla^2 f(x,y) = \frac{\delta^2 f(x,y)}{\delta^2 x^2} + \frac{\delta^2 f(x,y)}{\delta^2 y^2}, \tag{11}$$

where $a < x < b$ and $c < y < d$ and a, b, c, and d are image-area boundaries. Methods involving finite differences for solving boundary-value problems (Laplacian) consist of replacing each of the derivatives in the differential equation by an appropriate difference-quotient approximation. Partitioning the interval [a,b] into n equal steps of size h and [c,d] into m equal steps of size k provides a means of placing a grid on the rectangle a, b, c, d by drawing vertical and horizontal lines through the points with coordinates (x_i, y_j), where

$$\begin{aligned} x_i &= a + ih \text{ for each } i = 0,1,\ldots,n \\ y_j &= c + jk \text{ for each } j = 0,1,\ldots,m. \end{aligned} \tag{12}$$

The lines $x = x_i$ and $y = y_j$ are called the grid lines and their intersections are called mesh points of the grid [4]. For each mesh point in the interior of the grid, (x_i, y_j), $i = 1,2,\ldots,n-1$ and $j = 1,2,\ldots,m - 1$, the third-degree Taylor series can be expanded about the variable x and evaluated at x_{i+1} and x_{i-1} by

$$f(x_{i+1},y_j) = f(x_{i+h},y_j) = f(x_i,y_j) + hf'(x_i,y_j) + \tag{13}$$
$$h^2/2f''(x_i,y_j) + h^3/hf''' (x_i,y_j) + h^4/24f'''' (\beta_i,y_j),$$

where $x_i < \beta < x_{i+1}$, and

$$f(x_{i-1},y_j) = f(x_{i-h},y_j) = f(x_i,y_j) - hf'(x_i,y_j) + \tag{14}$$
$$h^2/2f''(x_i,y_j) - h^3/hf''' (x_i,y_j) + h^4/24f'''' (\tau_i,y_j),$$

where $x_{i-1} < \tau < x_i$. If these equations are added, the terms involving $f'(x_i)$ and $f'''(x_i)$ are eliminated, and algebraic manipulation gives,

$$\frac{\delta^2 f(x,y)}{\delta x^2} = \frac{1}{h^2} \mid f(x_{i+1},y_j) - 2*f(x_i,y_j) + f(x_{i-1},y_j) \mid$$
$$- \frac{h^2}{12} f''''(\phi,y_j) \tag{15}$$

for $x_{i-1} < \phi < x_{i+1}$. Similarly, the Taylor series can be used to generate the central-difference formula in the variable y about y_j resulting in

$$\frac{\delta^2 f(x,y)}{\delta y^2} = \frac{1}{k^2} \mid f(x_i,y_{j+1}) - 2*f(x_i,y_j) + f(x_i,y_{j-1}) \mid$$
$$- \frac{k^2}{12} f''''(x_i,\phi), \tag{16}$$

where $y_{j-1} < \phi < y_{j+1}$. Adding these terms, the Laplacian becomes

$$\nabla^2 f(x,y) = \frac{f(x_{i+1},y_j) + f(x_{i-1},y_j) - 2*f(x_i,y_j)}{h^2} + \frac{f(x_i,y_{j+1}) + f(x_i,y_{j-1}) - 2*f(x_i,y_j)}{k^2} - \frac{h^2 f''''(\phi,y_j)}{12} - \frac{k^2 f''''(x_i,\phi)}{12} \; . \tag{17}$$

However, if fourth-order derivatives are assumed negligible and h = k = 2, then the following commonly used image analysis technique for the Laplacian is derived,

$$\nabla^2 f(x,y) \approx f(x_i y_j) - 1/4 * [f(x_{i+1},y_j) + f(x_{i-1},y_j) + f(x_i,y_{j+1}) + f(x_i,y_{j-1})]. \tag{18}$$

The Laplacian is approximated for every x,y pair in the image. (It should be noted that this is a two-dimensional operator and image data can be averaged into a single image profile after Laplacian application to make presentation of results similar to those from other procedures.)

Figure 9a shows the results from applying this operator on a noise-free image. Scanning from pixel locations 1 through 10, it is demonstrated that the operator reads 0 until the edge is approached at pixel 10. At this location, the approximation identifies the edge location by a sharp intensity increase.

It is cautioned in Reference 5 that the Laplacian approximation tends to become ineffective when utilized on noisy images. To verify the effect of image noise on these results, the profile shown

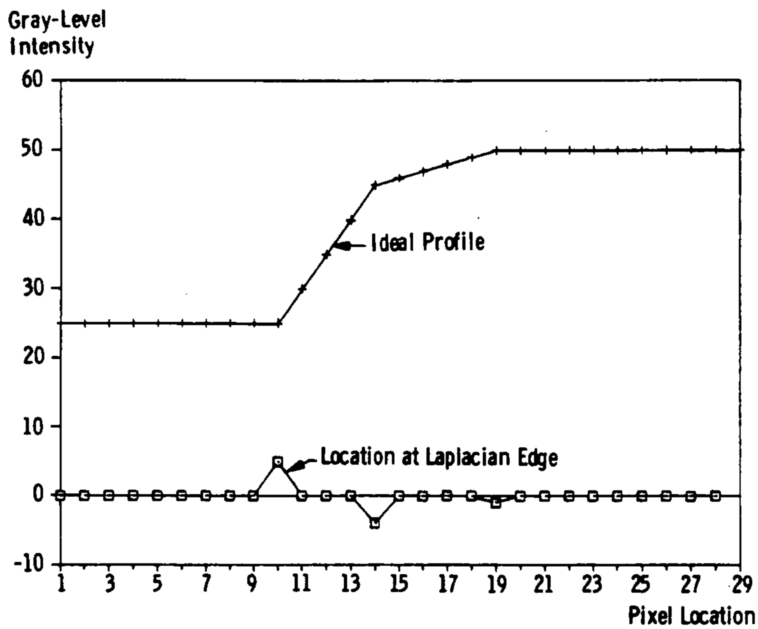

a. Ideal image

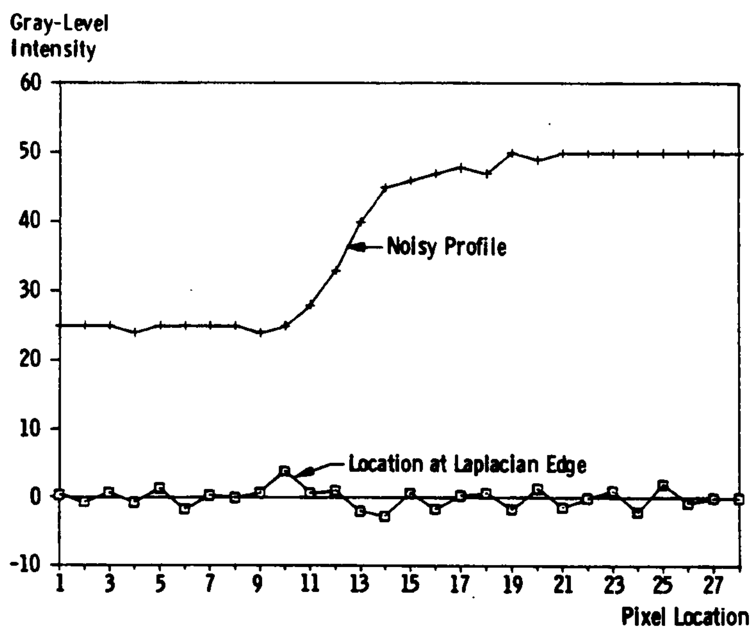

b. Noisy image

Figure 9. Example of the Laplacian operator.

in Figure 9b was analyzed. This profile is the average of four slightly different image profiles. The Laplacian approximation was evaluated using each of the four profiles. These results were then averaged producing the Laplacian result presented in Figure 9b. Although an edge can still be identified at pixel 10 in this noisy image, it can be concluded that additional image noise might prevent this operator from selecting the proper edge.

In summary, the edge detectors to be tested using the rocket nozzle throat simulator data described in Chapter III are edge detection by thresholding, and K-means and ISODATA clustering techniques as applied to an image profile. Additionally, the gradient and Laplacian approximations will be applied to a two-dimensional image area and subsequently averaged into an image profile.

CHAPTER III

EDGE DETECTION EXPERIMENTS

Rocket Nozzle Simulator

The logical process for determining which of the edge detection techniques previously discussed yields the best results on X-ray images was to acquire a reference image data set and compare the dimensions given by each of the edge detection techniques with the actual model dimensions. For this task, a nozzle simulator was designed and constructed from which X-ray images could be made for exactly known "throat" or hole diameters. One of the considerations in design of a simulator is that during a rocket motor firing, the nozzle throat becomes larger as hot gases from the burning propellant are expelled. A realistic simulator also should allow for simulation of different amounts of propellant loading while accounting for incremental increased throat (hole) diameters.

An X-ray beam becomes attenuated as it passes through a known thickness (x) of material defined by

$$I = I_0 * e^{-\mu X}, \tag{19}$$

where I_0 is the intensity at the detector with no absorber, and μ is the linear attenuation coefficient for each of the various materials at the given X-ray energy [7]. Since the density and attenuation coefficient were known for many materials including Lucite® and lead, rocket propellant and nozzle thickness were simulated by an appropriate amount of these materials.

The simulator was a 0.5-inch thick Plexiglas® box containing a series of metal plates with varying diameter holes (Figure 10). The box was approximately 24 inches long and 15 inches in height and width. Solid lead or Lucite® plates could be added in front or behind the varying throat sections to simulate a predetermined propellant loading. For this research, propellant simulations ranged from zero to approximately 15 inches.

Figure 11 shows the details of the throat simulator sections. Plates 1 through 14 were aluminum blocks 14 inches in height and ranging from a 0.5- to 1.0-inch thickness and a 3.0- to 5.0-inch width. A different sized hole was cut in the center of each plate, as shown by the dashed lines in Figure 11. The hole diameters in plates 5 through 14 only changed a total of about 0.5 inch. The amount of material through which X rays traveled was designed to be constant at 3 inches. This was obtained by adjusting the widths of plates 2 through 4, thus avoiding contrast changes in the image. Since the rocket throat "grows" as the firing progresses, the smallest hole (plate number 4) was used as a pretest "known" measurement. A ratio is set up between the number of pixels which represent the 1-inch reference hole as compared to the number of pixels between test hole edges. Therefore, a simple ratioing technique is used to determine "eroded" hole diameters. Analysis of edge detectors' performance was based on how accurately the hole sizes could be estimated.

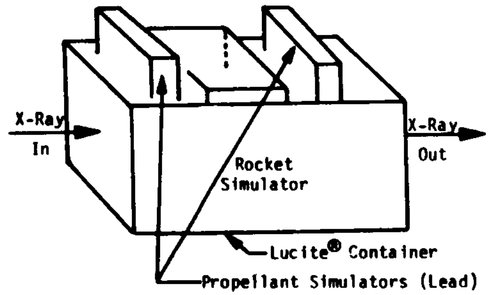

a. Overview

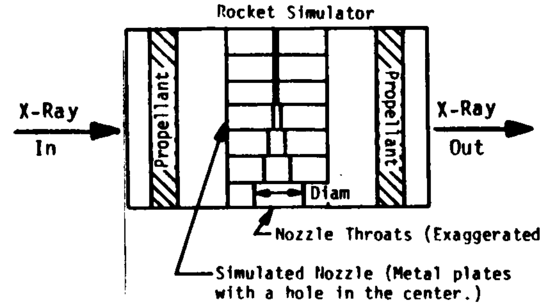

b. Top view of simulator

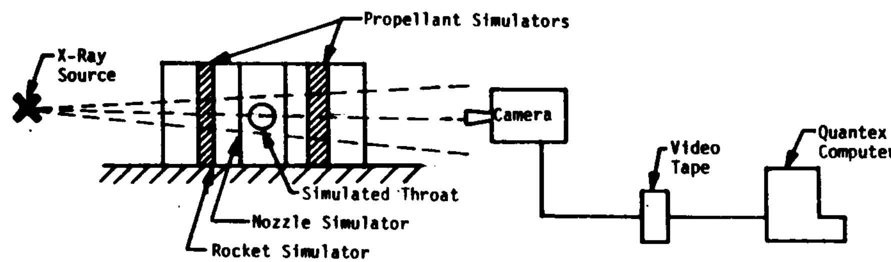

c. Side view of simulator

Figure 10. Overview of nozzle throat simulator.

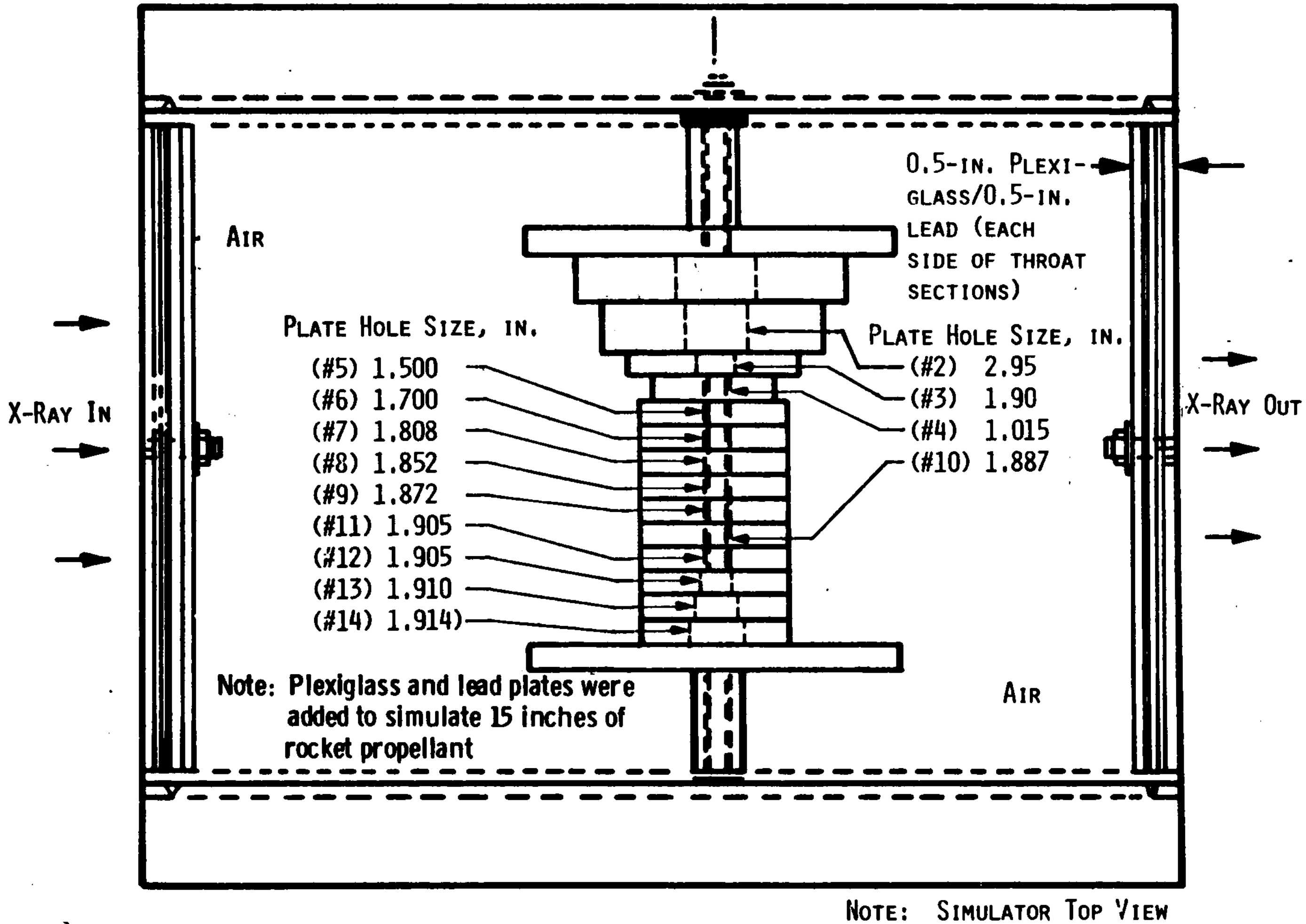

Figure 11. Details of simulated throat sections.

Images of the throat model were affected by the amount of propellant simulated and the nonlinear distribution of X-ray energy emitted from the source used. The more material added between the source and camera, the more X-ray energy is required to get the same gray-level intensity values on the image. Since a 6 MeV X-ray source was used for these experiments, model images became drastically darker as more propellant was simulated. Additionally, an ideal X-ray point source would emit a symmetric energy distribution radiating in a conical pattern toward the object. However, since this is a source of finite width, the energy distribution is not completely symmetric resulting in contrast changes in the image. Additional image noise is a result of X-ray scatter from the object as noted in Chapter I.

Nozzle Throat Data

The nozzle throat simulator was initially configured as shown in Figure 11, except no lead or Plexiglas® sheets were used to simulate motor propellant. A 6 MeV X-ray source provided 250 Rad/min at 1 meter from the source. The source to object and object to camera distances were 12.7 and 1.3 feet, respectively. The setup designated as Setup 1A in Table 1 produced the primary data from which edge detection results were judged. Other image recording configuration distances (Setups 1B, 2A, and 2B) are also given in Table 1. The images from Setups 1B, 2A, and 2B were used as a final test for those techniques which produced best results from the Setup 1A image.

Table 1. X-Ray Setup.

	Setup 1A	Setup 1B	Setup 2A	Setup 2B
x(ft)	1.3	7	1.3	7
y(ft)	12.7	7	12.7	7
Simulated Propellant Loading	None	None	11 Inches	15 Inches

Note: The distance between X-ray source and object is y, and x indicates the distance between object and camera.

Magnified 2x images were produced by adjusting the source-to-object and the object-to-camera distance so that they would be equal. The only difference between setups 1 and 2 was the addition of simulated propellant loading.

Analysis Hardware

Video images of the throat model were recorded on video tape, digitized by means of a Quantex® image processor, and stored on "floppy" disk. The images were displayed using an IBM PC/AT® and image-area data of hole diameter edges were stored in spreadsheet (LOTUS®) files. Laplacian and gradient approximations were analyzed using spreadsheet programming, and the other procedures which required more extensive software programming utilized these spreadsheet files as inputs.

Figure 12 shows a schematic of an image area which encompasses several edges that were selected for edge-detection technique analysis. Each image area consisted of 640 rows and 480 columns. For all of these analyses, a smaller area containing an edge similar to that shown in Figure 12 and labeled "A" was selcted by visual inspection and stored in a LOTUS® data file. The nominal area size was 5 pixels wide by 60 pixels high. For all procedures except gradient and Laplacian, the nominal 5-pixel width was averaged into a single column of data to reduce image spatial noise prior to edge detection (referred to as an image profile). Little or no edge detection accuracy was compromised with this procedure because averaging was performed parallel to the edge as indicated on Figure 12.

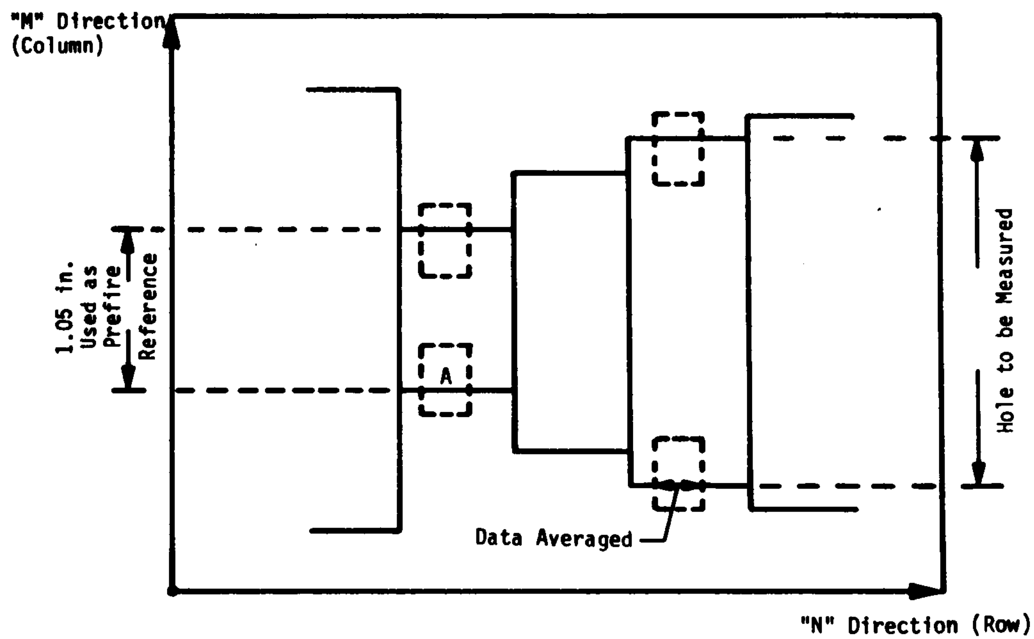

Figure 12. Example of an image area selection.

On the other hand, gradient and Laplacian operators used the entire 5 by 60 pixel area, and these results were averaged into a single column of profile data. Analysis was limited to about a 5-pixel width (5 by 60 area example) because the typical object width was only 8 to 10 pixels for Setup 1A. This was because the model was designed to simulate an entire rocket-firing erosion profile with a single image. Since the various hole diameters were designed to be viewed at the same time, the number of pixels that could be used to characterize any single hole was small. During an actual rocket firing, a larger area would be available for edge detection analysis and more data could be used to reduce the effects of image noise. It is estimated that for an actual rocket firing, an area width greater than 8 to 10 pixels could be averaged into a single column of data. This increase in number of pixels available for noise reduction would improve the reliability of edge detection results.

CHAPTER IV

EXPERIMENTAL RESULTS

Thresholding

Figure 13 presents a histogram of the pixel values along the profile of the 1.5-inch hole. As shown in Chapter II, thresholding requires a bimodal gray-level distribution for most effective application. As viewed in Figure 13, this profile does not have a bimodal distribution of gray-level data. For instance, gray-level ranges 120 through 129, 130 through 139, 150 through 159 each have more than 40 image pixels. In fact, inspection of the histogram data reveals the difficulty in selecting the mean dark pixels. If the 120 through 129 region is selected as mean dark because of its amplitude, then the 150 through 159 region could be considered mean light because of its amplitude also. However, from inspection of raw-image data, it is known that object pixels encompass the 190 through 209 gray-level range. Chapter II identified that a bimodal gray-level distribution is essential for this detection technique. Since this profile, which was typical for the data sets recorded, illustrates that no such distribution existed. This procedure was not considered as a candidate edge detector.

K-Means Pixel Clustering

The K-means clustering technique was presented in Chapter II. Table 2 presents three different results for measuring the 1.5-inch

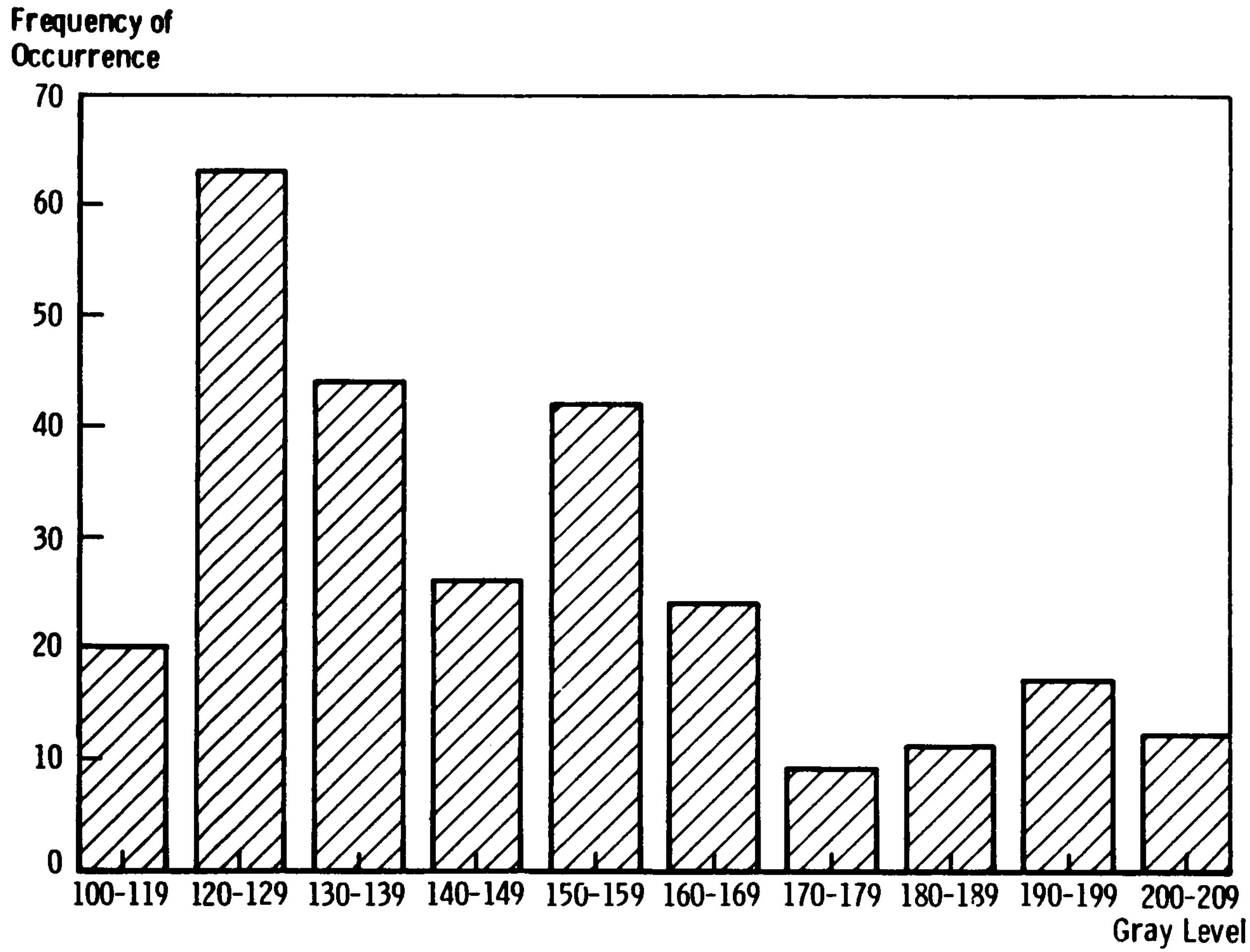

Figure 13. Gray-level histogram for 1.5-in. hole.

Table 2. Effect of Image-Area Selection in K-Means.

Hole Size (In.)	First Edge Area (From Graphic)	Computed Results (In.)	Error	
			Δ(In.)	Δ(%)
1.500	A*	1.624	+0.124	+8.3
1.500	B*	1.479	-0.021	-1.4
1.500	C*	1.334	-0.166	-11.1

* See Figure 14.

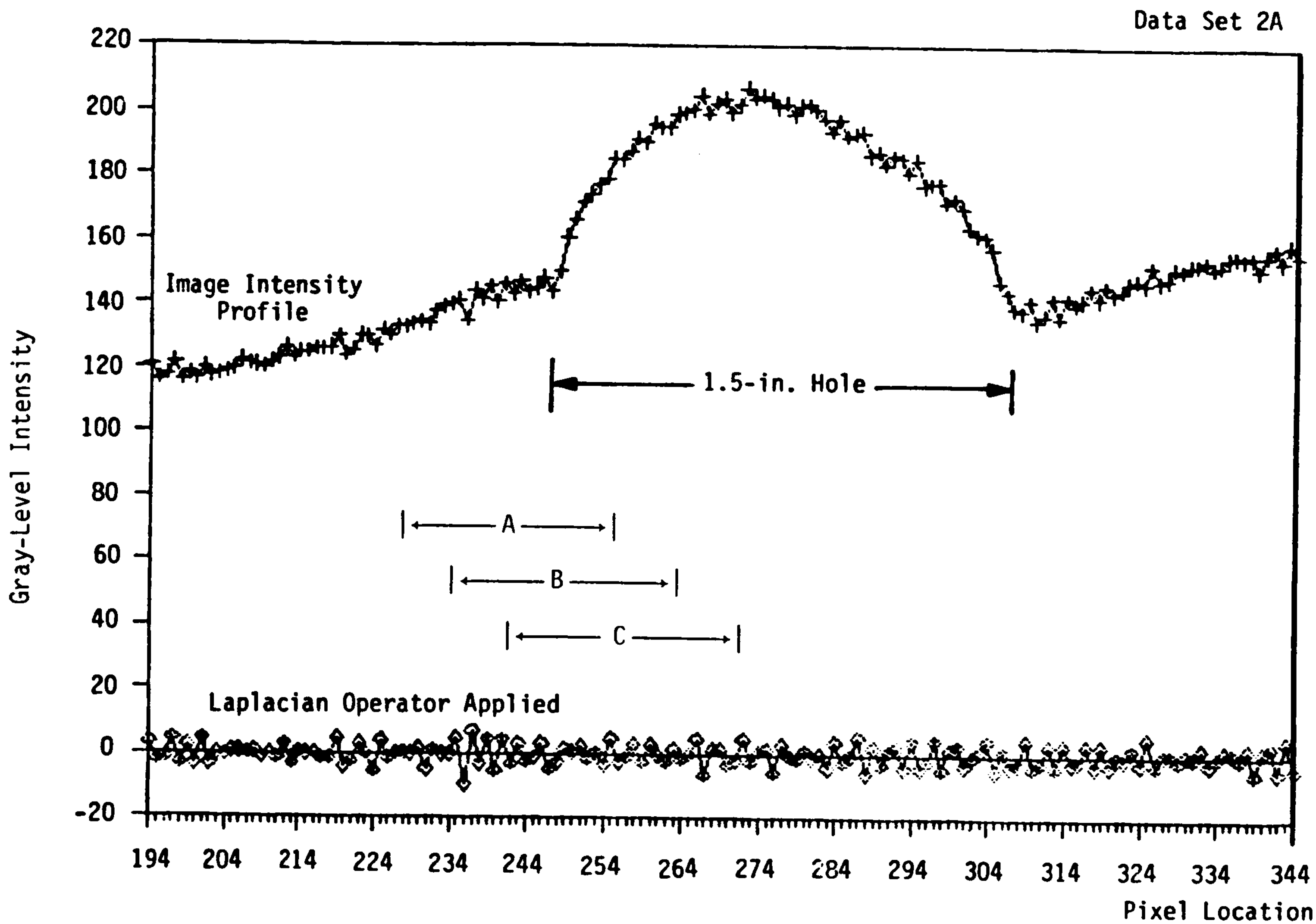

Figure 14. Application of Laplacian operator.

hole. After experimentation it was determined that the K-means result will vary for slightly different variations in image-area selection. Since K-means is a least-squares procedure, it will always produce a performance-index result regardless of the data input. The three results presented for the 1.5-inch hole come from the three logical choices for selection of the area containing the holes first edge (shown as pixel groupings A, B, and C in Figure 14). Although only a 0.29-inch difference exists between answers, when it is considered that at least as much variation could exist in selection of the second edge area for this hole, the total possible variance may be dramatically increased. Hence, meaningful results from this procedure is best obtained when a standard for edge area selection can be established. This was accomplished using another edge detector and will be discussed later.

ISODATA

Like the K-means, ISODATA results are dependent upon the image area selected for analysis. Therefore, a standard for data selection must be established for repeatable and meaningful results. An acceptable procedure was established and results of ISODATA together with a preprocessing technique will be presented later in this thesis.

Gradient

Sobel gradient edge detection results from the throat simulator data (Setup 1A) are presented in Table 3. These results show that the 2.95-inch hole is measured to within 0.264 inches. Accuracy in

Table 3. Gradient Results (Sobel).

Data Set 1A			
Known Hole Size	Computed Results (In.)	Difference Between Actual and Computed (In.)	Error (%)
1.500 in.	1.579	0.079	+5.2
1.700 in.	1.804	0.104	+5.8
1.808 in.	1.917	0.109	+6.0
2.950 in.	3.214	0.264	+8.9

measurement ranges from 8.9 percent for the 2.95-inch hole to 5.2 percent for the 1.5-inch hole. This method produces results with a slightly larger measurement error than does K-means. To determine the effect of image degradation, the image with 11 inches of simulated propellant loading and with minimal object magnification (Table 1, Setup 2A, page 31) was analyzed using the Sobel operator. These results are presented in Table 4. Because the image was degraded by the simulated propellant which reduced contrast and made the object more difficult to separate from the background, the results are not surprising. The average error increased to about 18 percent, and the scatter in measurement results for the various hole sizes increased to about 11 percent. This shows that the gradient is very much affected by image degradation. Since the K-means method will be shown to be relatively unaffected by the simulated propellant loading, either in accuracy or scatter results, the gradient technique was not further researched.

Laplacian

Figure 14 presents Laplacian output for the 1.5-inch hole. Since there are no clear peaks for the second derivative, no edge can be detected using this procedure (Figure 14). Although inspection of the one-dimensional image profile shown might suggest that a derivative operator should detect an edge between pixels 247 and 248, such is not the case. This is because the Laplacian represents results from an area of image data adjacent to the pixel locations

Table 4. Gradient Results for a Degraded Image.

Data Set 2A			
Known Hole Size	Computed Results (In.)	Difference Between Actual and Computed (In.)	Error (%)
1.500 in.	1.842	0.342	+22
1.700 in.	2.050	0.350	+21
1.808 in.	2.140	0.332	+18
2.950 in.	3.276	0.326	+11

and not just the 1-d profile shown in Figure 14. Since each pixel analyzed represents an area of neighboring pixels (as described in Chapter II), the hole profile presented in Figure 14 is not representative of the average image surface characteristics. Therefore, the intensity change between pixels 247 and 248 would not be reflected in the 2-d Laplacian output unless the neighboring profiles used in evaluation also reflected the intensity change at the same image locations. Although this is the case in a noise-free image, it seldom occurs with real data and the attendant noise in real-life images causes results such as those shown in Figure 14, and the procedure fails. The Laplacian was, therefore, dropped as a candidate edge detection procedure.

K-Means with Gradient

The K-means (and ISODATA) techniques could potentially be improved by using a standard procedure for image-edge region definition. Analysis of the Sobel gradient verified that it will result in identifying the approximate edge locations for each hole image. Additionally, its results cannot be influenced since no human judgment about image-edge region selection is required because the gradient is applied over the entire image as opposed to just a segment of the image profile as with the K-means method. Therefore, the gradient technique was used in conjunction with K-means to identify the edge location. The image-edge region consisted, by arbitrary definition, of 30 pixels on either side of the gradient edge. For example, if a gradient edge was found to be at pixel location 256, then pixels 226 through 286 were analyzed by K-means. Since the gradient will always yield the same result for the region around the image edge, it was postulated that use of this procedure with K-means should also yield a consistent result.

The results of the K-means technique incorporating the gradient area selection procedure on image Setup 2A is presented in Table 5. The largest error was in the measurement of the 2.950-inch hole. This error was 0.121 inches or a 4.1-percent error. Image pixel resolution is about 0.025 inches based on the number of pixels making up the known 1-inch reference hole, so this maximum error will correspond to about 5 image pixels. For the other hole measurements, the error was less than 0.10 inches. Since results comparable to those from gradient detection alone were obtained from the primary image, the other images (degraded, magnified) were analyzed. Table 6 compares previous results (data set 1A) with those images degraded by propellant simulation and magnified images. For the degraded image with no magnification, the measurement errors are comparable to those for the previous image. Maximum error is slightly higher (0.138 inches) but results for all measurements are much better than those from the gradient alone. Table 6 also shows that object magnification has no apparent impact on K-means results for either the normal or the degraded image. No errors greater than 0.127 inches are encountered from analysis of these magnified holes.

Table 5. K-Means Results.

Data Set 1A			
Known Hole Size	Computed Results (In.)	Difference Between Actual and Computed (In.)	Error (%)
1.500 in.	1.560	0.060	+4.0
1.700 in.	1.718	0.018	+1.1
1.808 in.	1.848	0.040	+2.2
2.950 in.	3.071	0.121	+4.1

Table 6. K-Means Results for Magnified and/or Degraded Images.

					Object Magnified by 100%			
	Data Set 1A		Degraded Image (2A)		Data Set 1B		Degraded Image (2B)	
Known Hole Size (In.)	Computed Results (In.)	Error	Computed Results (In.)	Error	Computed Results (In.)	Error	Computed Results (In.)	Error
1.500	1.560	Δ = 0.060" (+4.0%)	1.486	Δ = 0.014" (-1.4%)	1.373	Δ = 0.127" (-8.5%)	1.439	Δ = 0.061" (-4.1%)
1.700	1.718	Δ = 0.018" (+1.19%)	1.838	Δ = 0.138" (+8.1%)	1.702	Δ = 0.002" (+0.1%)	1.614	Δ = 0.086" (-5.0%)
1.808	1.848	Δ = 0.040" (+2.2%)	1.720	Δ = 0.088" (-4.9%)	1.851	Δ = 0.043" (+2.4%)	1.809	Δ = 0.001" (0.06%)
2.950	3.071	Δ = 0.121" (+4.1%)	2.873	Δ = 0.077" (-2.6%)	3.060	Δ = 0.110" (+3.7%)	*	---

* Out of field of view after image magnification.

ISODATA Pixel Clustering with Sobel Gradient

Because of the effectiveness found in using the K-means operator combined with the Sobel gradient, the second pixel clustering technique, ISODATA with the Sobel gradient was checked as a comparison. The results of ISODATA combination are presented in Table 7. A standardized method for image-area input selection must be established prior to analysis. Just as for K-means, the Sobel gradient was first used to identify the approximate edge location, then the ISODATA procedure was used to select an updated result based on the 60 pixels surrounding the gradient edge. By using this procedure, ISODATA produces about the same results as K-means. The error in measuring the 1.700-inch hole is 0.091 inches (-5.4% error) for ISODATA/Sobel gradient and only .018 inches (+1.1% error) for K-means/ Sobel gradient. The results of both methods compare closely for the other measurements shown. Since no apparent increase in accuracy was achieved by using this procedure, no further analysis was made.

K-Means Versus Visual Inspection

Finally, the K-means/Sobel gradient results are compared to those obtained by human visual inspection for the same image data. For the 1-inch reference hole data profile presented in Figure 15, the object edges are selected by visual inspection to be located at pixels 249 and 293 based on the consistent intensity change occurring after pixel 249 and before pixel 293. Using this same logic,

Table 7. ISODATA Detection Results.

True Hole Size (In.)	Data Set 1A	
	K-Means	ISODATA
1.500	1.560 (+4.0%)	1.436 (-4.3%)
1.700	1.718 (+1.1%)	1.609 (-5.4%)
1.808	1.848 (+2.2%)	1.733 (-4.1%)
2.950	3.071 (+4.1%)	2.921 (-1.0%)

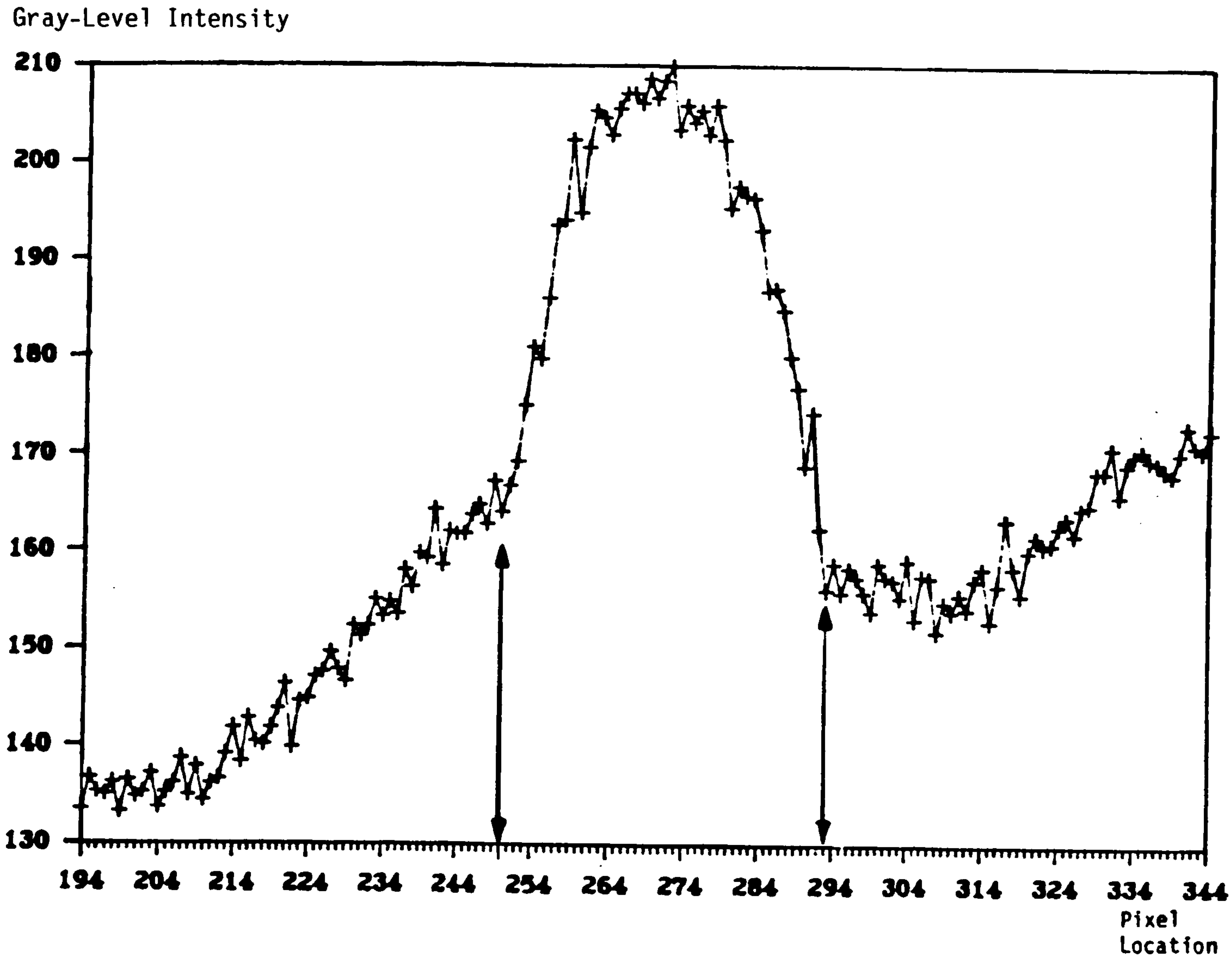

Figure 15. Edge detection by visual inspection.

the other hole edges were selected and the distance between the 1-inch hole edge was compared to the other hole image distances. The results of this comparison are presented in Table 8 along with those previously presented for the K-means/Sobel gradient method. These results show that the K-means/Sobel gradient method is about as accurate as image analysis by visual inspection since the error in hole measurement shown is about the same. Additionally, K-means results will always be the same for each image analyzed because of the structure of the analysis procedure, which is a major advantage of the K-means/Sobel gradient procedure over visual inspection. Visually, each image inspector will have an independent interpretation of edge locations. The K-means procedure produces consistent image analysis results from which an uncertainty in measurement can be estimated.

Table 8. Computer Versus Visual Results.

	Data Set 1A	
True Hole Size (In.)	K-Means	Results from Visual Inspection
1.500	1.560 (+4.0%)	1.450 (3.3%)
1.700	1.718 (+1.1%)	1.619 (4.8%)
1.808	1.848 (+2.2%)	1.740 (3.8%)
2.950	3.071 (+4.1%)	2.948 (0.07%)

CHAPTER V

CONCLUSIONS

The goal of this study was to evaluate edge detection techniques for radiographic image measurement. Based on the analysis of the experimental results with candidate procedures, the following conclusions were made.

Edge Detection by Thresholding

The edge detection by thresholding method outlined herein can be utilized as an image edge detector provided a bimodal gray-level distribution of image data is analyzed. The throat simulator images used for this study did not have such a distribution; therefore, the technique was dismissed as a candidate procedure.

K-Means Pixel Clustering

The K-means pixel clustering technique could not be used unless a standard for image-data area selection was established. Without such standardization, this procedure does not yield repeatable or meaningful results.

K-Means Pixel Clustering/Sobel Gradient Procedure

The K-means pixel clustering combined with the Sobel gradient preprocessing procedure was used to measure simulated nozzle throat hole diameters. The largest error in measurement (0.138 inches) was for the 1.700-inch hole recorded on a decreased contrast image simulating 15 inches of rocket propellant. Object magnification has no apparent effects on K-means/Sobel gradient results. The results are apparently as good as those based on visual analysis of image profile data. The K-means and Sobel graidnet techniques combined together were found to yield the most accurate and consistent results. Therefore, this approach is recommended for future application for nozzle throat edge detection and measurement.

ISODATA Pixel Clustering

The ISODATA pixel clustering procedure could not be used unless a standard for image-data area selection was established. Without standardization, this procedure does not yield repeatable or meaningful results.

ISODATA Pixel Clustering/Sobel Gradient Procedure

The ISODATA pixel clustering combined with Sobel gradient preprocessing technique provided results similar to those provided by the K-means/Sobel gradient method. Measurement error in analyzing a simulator image with no rocket propellant simulation was 0.091 inches for the 1.7-inch hole compared to 0.018 inches obtained by the K-means/Sobel gradient technique for the same hole. The combination of these two techniques also seems to be an appropriate analysis method for nozzle throat edge detection and measurement.

Gradient Edge Detection

The gradient edge detection technique was found to effectively locate simulator image edges. Its accuracy was comparable to the K-means/Sobel gradient procedure for images with no propellant loading. The maximum error was 0.264 inches for the 2.95-inch hole. Unfortunately, this procedure produces unsatisfactory results for low-contrast, rocket-propellant simulated images. Error for the same 2.95-inch hole increased to 0.326 inches.

Laplacian Edge Detection

This study showed how image noise hampers Laplacian edge detection. Given an image with little or no X-ray scatter or instrumentation noise, this procedure can be used to detect edges. However, for the throat simulator edges, no edge can be detected from the application of the Laplacian operator.

LIST OF REFERENCES

LIST OF REFERENCES

1. Barrett, H. H. and W. Swindell. Radiological Imaging. New York: Academic Press, 1981.

2. Gonzalez, R. C. and P. Wintz. Digital Image Processing. Reading, Massachusetts: Addison-Wesley, 1977.

3. Davis, L. S., A. Rosenfeld and J. Weszka. "Region Extraction by Averaging and Thresholding," IEEE Trans. Systems, Man., and Cybernetics, pp. 383-388, May 1975.

4. Tou, J. T. and R. C. Gonzalez. Pattern Recognition Principles. Reading, Massachusetts: Addison-Wesley, 1974.

5. Ballard, D. H. and C. M. Brown. Computer Vision. New Jersey: Prentice Hall, 1982.

6. Prewitt, J. M. S. In Picture Processing and Psychopictorics, B. S. Lipkin and A. Rosenfeld (Eds.). Cambridge, Massachusetts: MIT Press, 1976.

7. Burden, R. L., J. D. Fairs, and A. C. Reynolds. Numerical Analysis. Boston, Massachusetts: Prindle, Weber & Schmidt, 1981.

8. Heffan, H. and B. J. Brunty. High-Energy X-ray Applications for Nondestructive Testing. Palo Alto, California: Varian Associates, 1982.

VITA

A. L. Nasser was born on March 28, 1960, in Paris, Illinois. He attended classes at Rose-Hulman Institute of Technology in Terre Haute, Indiana, where he received a Bachelor of Science degree in Mechanical Engineering in May 1982.

In July 1982, he was employed by Sverdrup Technology, Inc., as a Project Engineer at the Arnold Engineering Development Center (AEDC). His duties included testing and research of rocket propulsion systems. He accepted a marketing position at the Sverdrup corporate headquarters in Nashville, Tennessee, in the Spring of 1988, and he is presently Senior Proposal Manager for Sverdrup Corporation Southern Group.

Mr. Nasser attended classes at The University of Tennessee Space Institute from September 1982 until August 1988, and earned a Master of Science degree in Engineering Science from The University of Tennessee, Knoxville. Mr. Nasser's thesis committee was composed of Dr. Ronald Belz (chairman), Dr. Jack Hansen, and Dr. Chad Limbaugh.